nature water

Article

https://doi.org/10.1038/s44221-024-00232-7

Near-complete destruction of PFAS in aqueous film-forming foam by integrated photo-electrochemical processes

In the format provided by the authors and unedited

Table of Contents

Text S1. Details of density function theory calculation.

The calculation adopted the Marcus theory to estimate the activation enthalpy of these two structures to lose one electron, which simulates the PFAS destruction via direct electron transfer to the anode.[1] The calculation was performed on Gaussian 16 software.[2] Molecular geometry optimization and frequency calculation were conducted via B3LYP method on the 6-311+G(2d,2p) basis set. The solvation effect was considered by the SMD-water model. The model reduction reactions are

$$C_7F_{15}–COO\bullet + e^- = C_7F_{15}–COO^- \quad (S1)$$

$$C_7F_{14}H–COO\bullet + e^- = C_7F_{14}H–COO^- \quad (S2)$$

The free energy (G) of each optimized chemical structure was calculated and then yielded the free energy of the reaction ($\Delta_r G^\circ$). The standard reduction potentials (E°) of reactions S1 and S2 can be obtained by:

$$E^\circ = -\frac{\Delta_r G^\circ}{nF} - E^\circ_{abs} \quad (S3)$$

where, n = 1 is the number of electrons transferred; F (96485 C/mol) is the Faraday constant; E°_{abs} = 4.28 eV is the absolute standard hydrogen potential vs. free electron on a scale of the electron volt. The activation enthalpy (($\Delta H^\ddagger$) of reactions S1 and S2 as a function of anodic potential (E) can be expressed as

$$\Delta H^\ddagger = \frac{\lambda_H}{4}\left(1 - \frac{96.5(E-E^\circ)}{\lambda_H}\right)^2 \quad (S4)$$

where, λ_H is the total reorganization energy. It is calculated by subtracting the standard enthalpy of the radical ($C_7F_{15}–COO\bullet$ or $C_7F_{14}H–COO\bullet$) from that of its anionic form, maintaining the same geometry. **Fig. S1** was plotted by calculating $\Delta H^\ddagger$ at various anodic potentials (E vs. RHE) at a step of 0.2 V_{RHE}.

Text S2. Instrument setup for targeted and nontargeted PFAS analysis.

Targeted analysis of PFASs was performed on an ultra-performance liquid chromatograph (UPLC, Thermo Vanquish) coupled to a triple quadrupole mass spectrometer (QQQ MS/MS, Thermo Altis). 10 μL of the sample was injected and then separated on a Thermo Scientific Hypersil GOLD PFP column (2.1 mm × 100 mm, 1.9 μm), which was maintained at 40 °C. Chromatographic separation was carried out with 5 mM ammonium acetate in water (mobile phase A) and acetonitrile (mobile phase B) at a flow rate of 0.4 mL/min. The LC gradient was as follows: 0 min (20% B), 0.5 min (20% B), 3 min (80% B), 5 min (100% B), 5.5 min (100% B), 5.6 min (20% B) and 8 min (20% B). The MS parameters were optimized based on the selected reaction monitoring (SRM) transitions (precursor/product fragment ion pair). Sample acquisition was carried out with Thermo XCalibur 4.5 software, and data analysis was performed with Thermo TraceFinder 5.1 software.

Nontargeted analysis of PFAS transformation products and precursors was performed on high-performance liquid chromatography-quadrupole time-of-flight mass spectrometry (HPLC/QToF-MS, SCIEX). For HPLC separation, a 50 μL sample was loaded onto a Phenomenex Gemini

column (particle size 3 μm, 100 × 3 mm, Phenomenex) and eluted with ultrapure water (A) and methanol (B) (both amended with 5 mM ammonium acetate) at a flow rate of 0.6 mL/min, with the following gradient: 90% A−10% B at 0−1.5 min, 35% A − 65% B at 1.5−8 min, 5% A − 95% B at 8−8.1 min, 1% A − 99% B at 8.1−12.5 min, and 90% A −10% B at 12.5−15.5 min. Data acquisition was turned off for the first 3 min of the run to prevent salts from entering the detector. High-resolution mass spectrometry analysis was performed on a SCIEX X500 QToF mass spectrometer in dual electrospray ionization (ESI) negative mode. A SWATH acquisition method was used in LC-QToF-MS analysis in negative ion mode with ion spray voltage at −4500 V. The QToF-MS/MS was set to scan fragment ions (ranging from 50 − 2500 Da) for parent ion masses between 100-2500 Da.

The validation of polyfluorinated intermediates and precursors is based on the following criteria: (i) mass tolerance < 5 ppm; (ii) peak area > 10^2; (iii) peak area increased depart from time-zero.

Text S3. Characterization of photochemical reactor.

Photon flux, effective path length, and photon fluence rate of the UV reactor used in this study were obtained following reported protocols.[3,4]

Photon flux was determined by an iodide/iodate (I^- /IO_3^-) actinometer at 254 nm UV light (UV_{254}) irradiation. A 750 mL actinometer solution contained 0.5 M potassium iodide (KI) and 0.1 M sodium iodate ($NaIO_3$). Upon UV irradiation, triiodide (I_3^-) was generated. Its concentration was quantified by measuring the maximum absorbance at 352 nm and applying the molar extinction coefficient of 26400 $M^{-1}\cdot cm^{-1}$. Eq. S5 was used to calculate photon flux,

$$[I_3^-] = \frac{\Phi_{I_3^-} I_0}{V} t \quad \text{(S5)}$$

where $[I_3^-]$ is I_3^- concentration (M), I_0 is photon flux ($E\cdot s^{-1}$), t is time (sec), V = reactor volume (L), and $\Phi_{I_3^-}$ is the I_3^- formation quantum yield (0.74 $mol\cdot E^{-1}$). The slope obtained from plotting $[I_3^-]$ versus t was used to calculate the photon flux, I_0 as $1.3 \pm 0.2\times10^{-6}$ $E\cdot s^{-1}$ (**Fig. A1a**).

The effective path length was determined by hydrogen peroxide (H_2O_2) photolysis. Briefly, a 750 mL of 500 μM H_2O_2 solution was introduced to the UV reactor. H_2O_2 was quantified by the potassium titanium oxalate spectrophotometric method.[5]

It is known that the photolysis of H_2O_2 follows first-order kinetics,

$$\ln \frac{[H_2O_2]}{[H_2O_2]_0} = \left(\frac{-2.303 \varepsilon_{H_2O_2} Z_{eff} I_0 \Phi_{H_2O_2}}{V}\right) t \quad \text{(S6)}$$

where $\varepsilon_{H_2O_2}$ is H_2O_2 molar extinction coefficient (19.6 M^{-1} cm^{-1})[2.5], Z_{eff} is effective pathlength (cm), I_0 is photon flux ($1.3 \pm 0.2\times10^{-6}$ E s^{-1}), Φ_{H2O2} is H_2O_2 photolysis quantum yield (1 mol E^{-1}), and V is solution volume (0.75 L). The slope of $\ln[H_2O_2]/[H_2O_2]_0$ versus t can be used to calculate Z_{eff}, which is 27 cm (**Fig. A1b**).

The average photon fluence rate, I_{avg}, represents the incident intensity averaged over the entire solution volume. The value of 5.4×10^{-8} $E\cdot s^{-1}\cdot cm^{-2}$ was calculated based on equation S7.

$$I_{avg} = \frac{I_0 Z_{eff}}{1000V} \quad \text{(S7)}$$

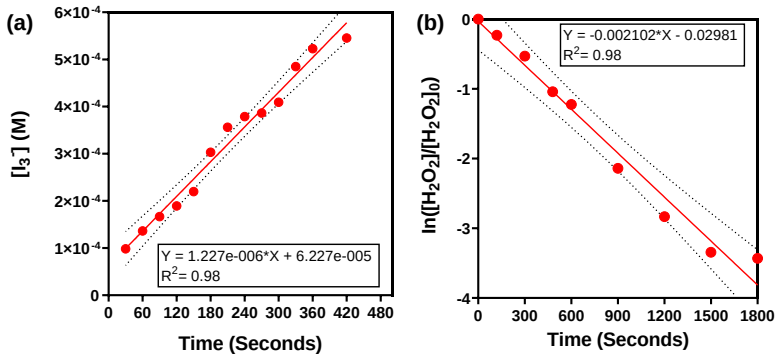

Fig. A1. (a) I_3^- generation during UV_{254} irradiation of the I^-/IO_3^- actinometer. Reaction conditions: $[KI]_0$ = 0.5 M, $[NaIO_3]_0$ = 0.1 M, light source: 16 W UV LP Hg lamp. (b) Photolysis of H_2O_2 throughout UV_{254} irradiation. Reaction conditions: $[H_2O_2]_0$ = 500 µM, light source: 16 W UV LP Hg lamp.

Table S1. Summary of available literature that reported total fluorine (TF) and defluorination efficiency (DeF) in AFFF treatment.

Approach	AFFF-Impacted Water	Max. Initial TF (mg/L)	TF quantification Method	Max. DeF	Refs
UV/S + EO	**Diluted AFFF**	**200**	**CIC**	**~100%**	**This study**
EO	Diluted AFFF	2.4	TOPA [a]	71%	[6]
EO	Still bottom of IDW [b]	27	^{19}F-NMR [c]	81%	[7]
EO	Diluted AFFF	NA.	TOPA	78%	[8]
Plasma	IDW	4.9	CIC	33%	[9]
UV/S	Diluted AFFF	0.16	^{19}F-NMR	50%	[4]
Hydrothermal	Diluted AFFF	6,650	^{19}F-NMR	~100%	[10]
Hydrothermal	Diluted AFFF	2,189	Estimated by identified PFAS	~100%	[11]

[a] Total oxidizable precursor assay. [b] Investigation derived waste. [c] Fluorine-19 nuclear magnetic resonance spectroscopy

Table S2. Properties of AFFF before and after being amended for treatment.

	Buckeye AFFF	**Ansulite AFFF**	**Buckeye Diluted by Tap Water [c]** (100-fold dilution; amended with 100 mM Na_2SO_3)	**Buckeye Diluted by Groundwater** (500-fold dilution; amended with 10 mM Na_2SO_3)	**Buckeye Diluted by ROC** (500-fold dilution; amended with 10 mM Na_2SO_3)
Conductivity (mS/cm)[a]	-	-	0.296	0.329	5.12
pH	9.7	9.1	Adjusted to 12 by NaOH	Adjusted to 12 by NaOH	Adjusted to 12 by NaOH
Total fluorine (mg/L)	10,100	6,100	102	21	21
Cl^- (mg/L)	ND[b]	ND	1.5	31	186
SO_4^{2-} (mg/L)	ND	ND	7.4	338	949
Background TOC of water matrices (mg/L)[d]	ND	ND	2.0	0.6	15.5

a The values are the conductivity of water matrices collected as it is. All water samples have a conductivity of 15.8 mS/cm at the stage of EO treatment due to the supplement of Na_2SO_3 at the stage of UV/S treatment (which was oxidized to Na_2SO_4 when EO started) and Na_2SO_4 before EO treatment.

b Not detected. Raw AFFF does not contain Cl^-, NO_3^-, and SO_4^{2-}.

c Buckeye AFFF was intentionally diluted by tap water, groundwater, and reversed osmosis concentrate. Cl^- and SO_4^{2-} were carried over from these matrices.

d The listed values are the intrinsic TOC of tap water, groundwater, and reverse osmosis concentrate. The background TOC values are insignificant compared with that of raw Buckeye AFFF product (188 g/L) and after 100-fold dilution (1882 mg/L).

Table S3. Full names, abbreviations, CAS registry numbers, method detection limit (MDL), and mean PFAS concentrations detected in the raw AFFF samples (#1: Buckeye 3%; #2: Ansulite 6%).

No.	Full name	Abbr.	CAS No.	RT (min)[a]	Blank (µg/L)	MDL (µg/L)	Mean Conc. (µg/L) #1	Mean Conc. (µg/L) #2
1	Perfluoro-n-butanoic acid	PFBA	375-22-4	0.77	ND[b]	0.004	61.3	731.7
2	Perfluoro-n-pentanoic acid	PFPeA	2706-90-3	0.67	ND	0.004	586.5	10.7
3	Perfluoro-n-hexanoic acid	PFHxA	307-24-4	2.07	ND	0.004	1763.2	216.6
4	Perfluoro-n-heptanoic acid	PFHpA	375-85-9	2.57	ND	0.004	32.4	12.7
5	Perfluoro-n-octanoic acid	PFOA	335-67-1	2.78	0.009	0.004	3543	42.6
6	Perfluoro-n-nonaoic acid	PFNA	375-95-1	2.96	ND	0.004	3.1	ND
7	Perfluoro-n-decanoic acid	PFDA	335-76-2	3.03	ND	0.004	7.5	ND
8	Perfluoro-n-undecanoic acid	PFUdA	2058-94-8	3.17	ND	0.004	ND	ND
9	Perfluoro-n-dodecanoic acid	PFDoA	307-55-1	3.29	ND	0.004	ND	ND
10	Perflluoro-n-tridecanoic acid	PFTrDA	72629-94-8	3.41	ND	0.004	ND	ND
11	Perflluoro-n-tetradecanoic acid	PFTeDA	376-06-7	3.53	ND	0.004	ND	ND
12	Potassium perfluoro-1-butanesulfonate	PFBS	375-73-5	1.35	ND	0.004	14.2	ND
13	Sodium perfluoro-1-pentanesulfonate	PFPeS	630402-22-1	2.4	ND	0.004	4.3	7.9
14	Sodium perfluoro-1-hexanesulfonate	PFHxS: linear	355-46-4	2.63	ND	0.004	17.9	ND
		PFHxS: branched			ND	0.004	8.3	ND
15	Sodium-perfluoro-1-heptanesulfonamide	PFHpS	375-92-8	2.78	ND	0.004	3	ND
16	Sodium perfluoro-1-octanesulfonate	PFOS: linear	1763-23-1	2.91	ND	0.004	31.2	12.7
		PFOS: branched			ND	0.004	11.4	10.1
17	Sodium perfluoro-1-nonanesulfonate	PFNS	98789-57-2	3.02	ND	0.004	1.3	ND
18	Sodium-perfluoro-1-decanesulfonate	PFDS	335-77-3	3.13	ND	0.004	ND	ND

19	Sodium 1H,1H,2H,2H-perfluorohexane sulfonate	4:2 FTS	757124-72-4	1.26	0.004	0.004	418.1	ND
20	Sodium 1H,1H,2H,2H-perfluorooctane sulfonate	6:2 FTS	27619-97-2	2.61	ND	0.004	139427.6	32055.0
21	Sodium 1H,1H,2H,2H-perfluorodecane sulfonate	8:2 FTS	39108-34-4	2.92	0.011	0.004	7852.7	ND
22	Sodium 1H,1H,2H,2H-perfluorododecane sulfonate*	10:2 FTS	N/A	3.18	ND	0.004	2.5	ND
23	Perfluoro-1-octanesulfonamide	FOSA-1	754-91-6	3.87	ND	0.004	ND	ND
24	Perfluoro-1-octanesulfonamidoacetic acid*	FOSAA	2806-24-8	3.2	ND	0.004	ND	ND
25	N-methylperfluoro-1-octanesulfonamidoacetic acid	N-MeFOSAA	2355-31-9	3.43	ND	0.004	ND	ND
26	N-methylperfluoro-1-octanesulfonamide*	N-MeFOSA-M	31506-32-8	4.36	ND	0.004	ND	ND
27	N-ethylperfluoro-1-octanesulfonamidoacetic acid	N-EtFOSAA	2991-50-6	3.48	ND	0.004	ND	ND
28	N-ethylperfluoro-1-octanesulfonamide*	N-EtFOSA-M	4151-50-2	4.45	ND	0.004	ND	ND
29	Trifluoroacetate	TFA	2923-18-4	0.46	ND	0.004	12.3	283.8
30	Perfluoropropanoic acid	PFPA	422-64-0	0.48	ND	0.004	6.8	1333.0

[a] Retention time in minutes. [b] Not detected.

Table S4. UV light absorbance at 254 nm.

Dilution ratios	**1 to 50**	**1 to 100**	**1 to 500**
$[TF]_0$ (mg/L)	21	103	200
Before*	1.36	0.36	0.03
After UV/S	0.36	0.33	0.04
After EO	0.29	0.12	0.03

* AFFF samples were measured as it after dilution without sulfite addition.

Table S5. Information of all PFAS chemicals used in this study.

No.	Chemical name	Abbr.	CAS No.	Purity (%)	Vendor
1	sodium trifluoroacetate	TFA	2923-18-4	97	Strem Chemicals
2	Perfluoropropionic acid	PFPA	422-64-0	98	TCI
3	Perfluorobutanoic acid	PFBA	375-22-4	98	Sigma-Aldrich
4	Perfluoropentanoic acid	PFPeA	2706-90-3	98	TCI
5	Perfluorohexanoic acid	PFHxA	307-24-4	98	TCI
6	Perfluoroheptanoic acid	PFHpA	375-85-9	97	Sigma-Aldrich
7	Perfluorooctanoic acid	PFOA	335-67-1	95	Sigma-Aldrich
8	Perfluorononanoic acid	PFNA	375-95-1	97	Sigma-Aldrich
9	Potassium nonafluoro-1-butanesulfonate	PFBS	29420-49-3	97	Sigma-Aldrich
10	Tridecafluorohexane-1-sulfonic acid potassium salt	PFHxS	3871-99-6	98	Frontier scientific
11	Heptadecafluorooctanesulfonic acid potassium salt	PFOS	1763-23-1	98	Sigma-Aldrich
12	1H,1H,2H,2H-Perfluorohexanesulfonic acid	4:2 FTS	757124-72-4	97	SynQuest
13	1H,1H,2H,2H-Perfluorooctanesulfonic acid	6:2 FTS	6164-3-49	97	SynQuest
14	1H,1H,2H,2H-Perfluorodecanesulfonic acid	8:2 FTS	39108-34-4	97	SynQuest

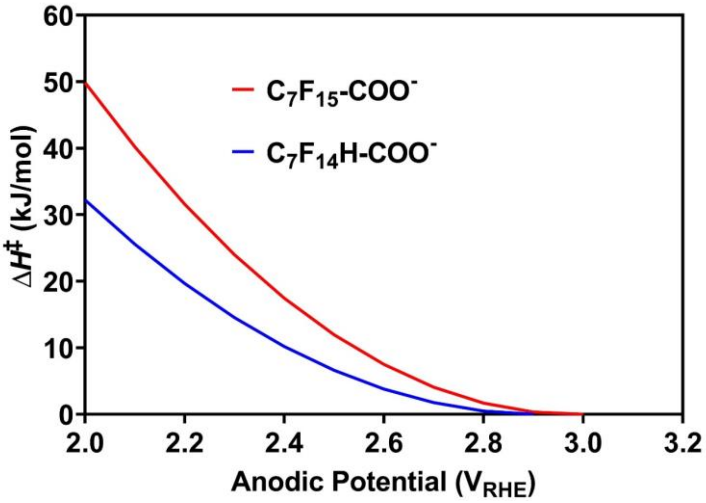

Fig. S1. The activation enthalpy (ΔH‡) for the target molecule to lose one electron as a function of anodic potential versus reversible hydrogen electrode (RHE).

Fig. S2. Photo to visualize the vigorous foam formation of Buckeye AFFF at 1 to 100 dilution treated by EO without UV/S pretreatment. The EO flow cell was operated at 5 A to treat 200 mL diluted AFFF to showcase the foaming.

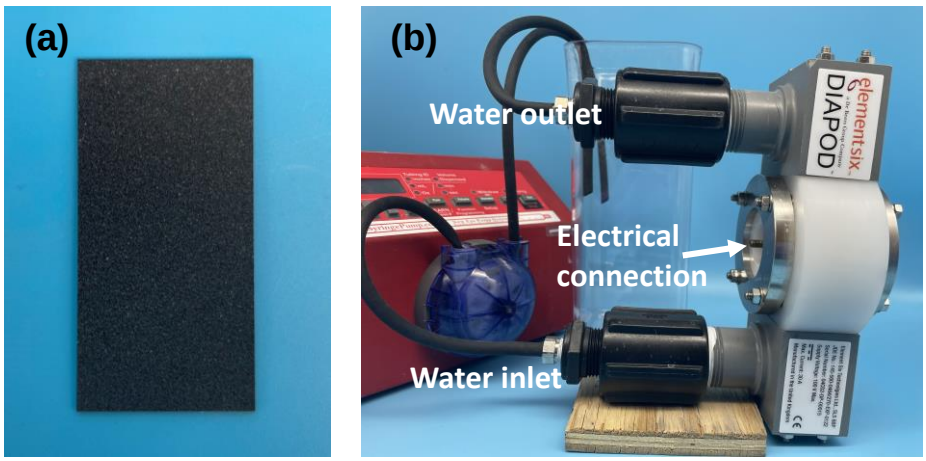

Fig. S3. Photos of (a) plate-type BDD and (b) BDD flow cell.

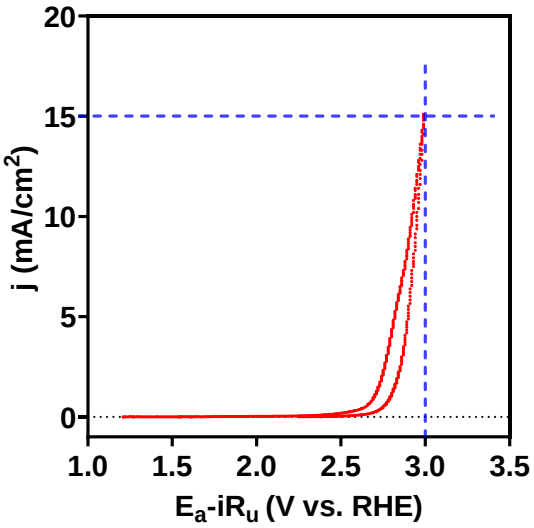

Fig. S4. Cyclic voltammetry of plate-type BDD electrode in 100 mM Na_2SO_4 electrolyte.

The anodic potential (E_a) was corrected by the product of total current (i) and uncompensated resistance (R_u). The R_u (= 0.3 Ω) was obtained by the impedance method at 100 kHz with a 20 mV sine wave.[12]

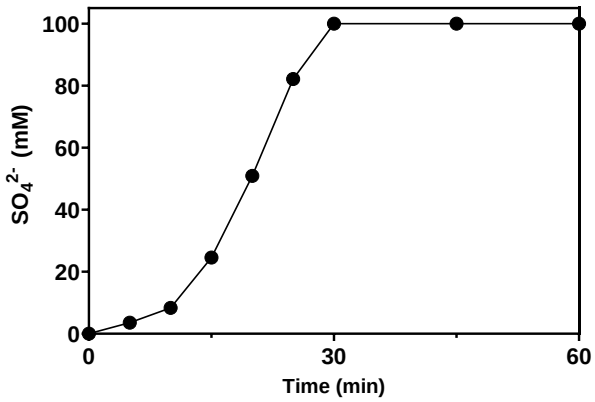

Fig. S5. Yield of SO_4^{2-} by the EO of 100 mM Na_2SO_3 electrolyte (20 mL) by a BDD anode (16 cm^2) at 15 mA/cm^2.

Sulfite (SO_3^{2-}) was readily oxidized to SO_4^{2-} within 30 min. This figure aims to show the vulnerability of SO_3^{2-} toward oxidation. Note that this is an extreme case assuming no loss of SO_3^{2-} in the UV/S process. We confirmed that, in the UV/S-EO tandem treatment of individual PFAS and AFFF-related samples, all residual SO_3^{2-} were oxidized to SO_4^{2-} in the initial 10 min of EO.

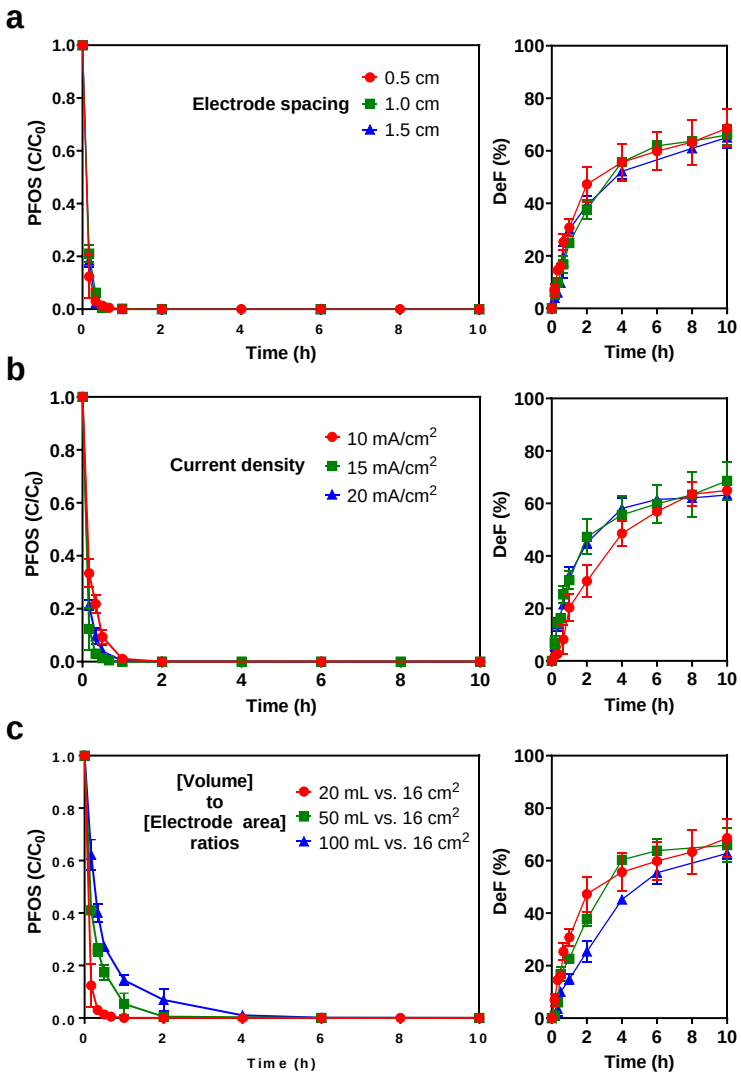

Fig. S6. Optimization of parameters including (a) electrode spacing, (b) current density, and (c) volume-to-electrode area ratios for PFOS destruction and defluorination. The electrolyte is 100 mM Na_2SO_4 spiked with 25 µM PFOS. Data are presented as mean values of triplicates ± standard deviation.

Electrode spacing did not have an impact on PFOS destruction and defluorination. Spacing smaller than 0.5 cm may cause the contact (i.e., short-circuiting) of the BDD and the stainless steel cathode; larger than 0.5 cm leads to an increase in cell voltage. Thus, the optimized spacing is determined as 0.5 cm. A current density higher than 15 mA/cm^2 did not further promote PFOS destruction and defluorination, as water splitting competed with the PFOS destruction reaction. The optimum current density is determined as 15 mA/cm^2. As for the [volume]/[electrode area] ratio, this parameter determines the required treatment duration but does not change the reaction mechanism. Therefore, we decided to use 20 mL electrolyte vs. 16 cm^2 BDD area as the optimum setup. It is important to emphasize that no matter how we adjusted the parameters, near-complete defluorination (~100 DeF%) of PFOS was not achieved. These results indicate that the incomplete defluorination of PFOS and other certain structures discussed in the manuscript was not a consequence of unideal operating conditions and reactor design.

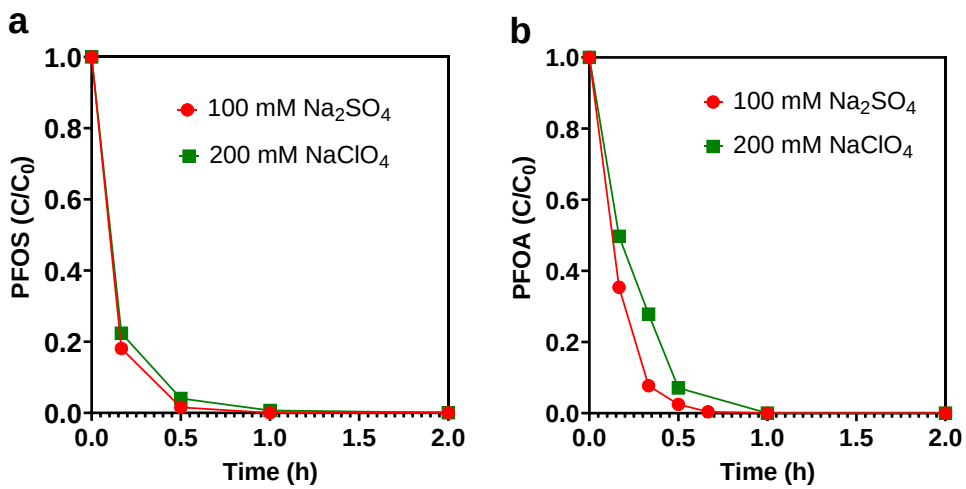

Fig. S7. EO treatment of (a) PFOS and (b) PFOA in 100 mM Na_2SO_4 and 200 mM $NaClO_4$ electrolytes (20 mL amended with 25 μM PFOS or PFOA). The current density was 15 mA/cm^2. BDD electrode area was 16 cm^2.

To further elucidate the roles of sulfate radicals, we compared the EO treatment of PFOS and PFOA in Na_2SO_4 and $NaClO_4$ (only HO• could be produced) electrolytes. As shown in Fig. S7, The destruction behaviors of PFOS were identical in Na_2SO_4 and $NaClO_4$ electrolytes. However, accelerated degradation of PFOA was observed in Na_2SO_4, echoing the promoting roles of SO_4^{-}• in PFCA destruction.

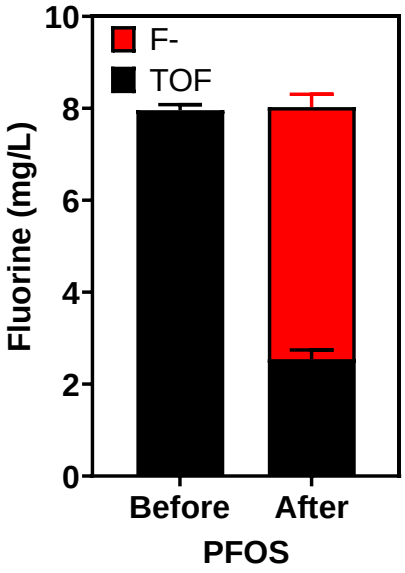

Fig. S8. Analysis of total organic fluorine (TOF) and fluoride in samples derived from the EO treatment of 25 μM PFOS before and after 8 h of EO treatment. The setup is the same as described in **Fig. 1** in the manuscript. Data are presented as mean values of triplicates ± standard deviation.

We combined combustion ion chromatography (CIC) and ion chromatography (IC) to quantify the total organic fluorine (TOF) and F^- of PFOS after 8 h of EO treatment (Fig. S8). The results indicate that the ~30% gap in DeF was indeed contributed by organofluorine. It is critical to note that targeted PFAS analysis confirmed that no short-chain PFCAs and PFSA were detected after 8 h of EO treatment. Thus, the remaining TOF should not be contributed by these targeted PFAS. Secondly, we are conducting suspect screening on high-performance liquid chromatography-quadrupole time-of-flight mass spectrometry (HPLC/Q-ToF-MS). While the investigation is still ongoing and could not be covered in this study, the candidate m/z signals do not match the hypothesized structure such as $^-OOC{-}(CF_2)_n{-}COO^-$ and $^-OOC{-}(CF_2)_n{-}SO_3^-$ (these structures were proposed assuming the tail group $-CF_3$ of PFCAs and PFSAs was subjected to C−F bond cleavage and hydrolysis and defluorination to $-COO^-$).

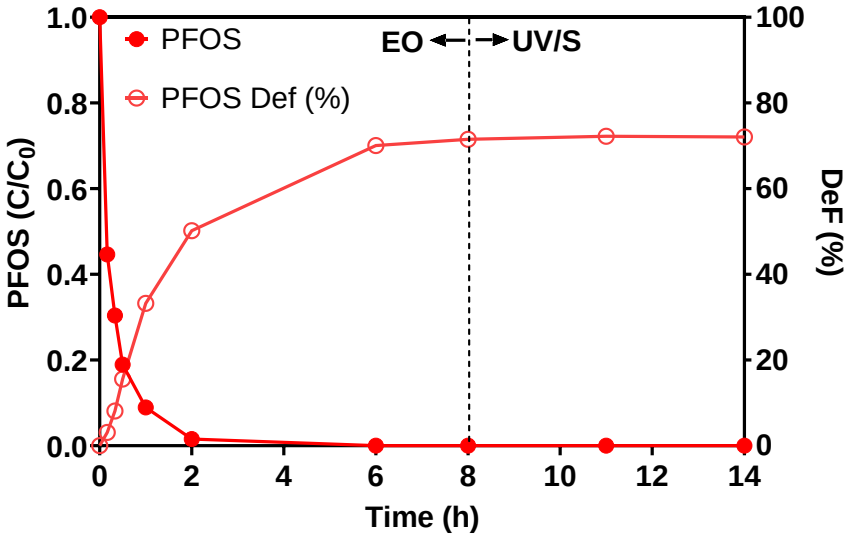

Fig. S9. Treatment of PFOS (25 μM) in 100 mM Na_2SO_4 electrolyte by EO followed by UV/S treatment. Before UV/S treatment, 10 mM Na_2SO_3 was added to the electrolyte.

The results show that unknown compounds generated from EO cannot be defluorinated by UV/S reduction. It is concluded that EO treatment of certain PFAS (n=3, 5, 7, 8) forms organofluorine products. The investigation on PFOS, as a representative n=8 PFAS, already reveals that the remaining organofluorine products are resistant to EO and UV/S reduction. The identification of product structures warrants further study. More importantly, these fundamental insights also highlight the urgency and importance of process innovation to avoid the formation of recalcitrant organofluorine and realize ~100% defluorination.

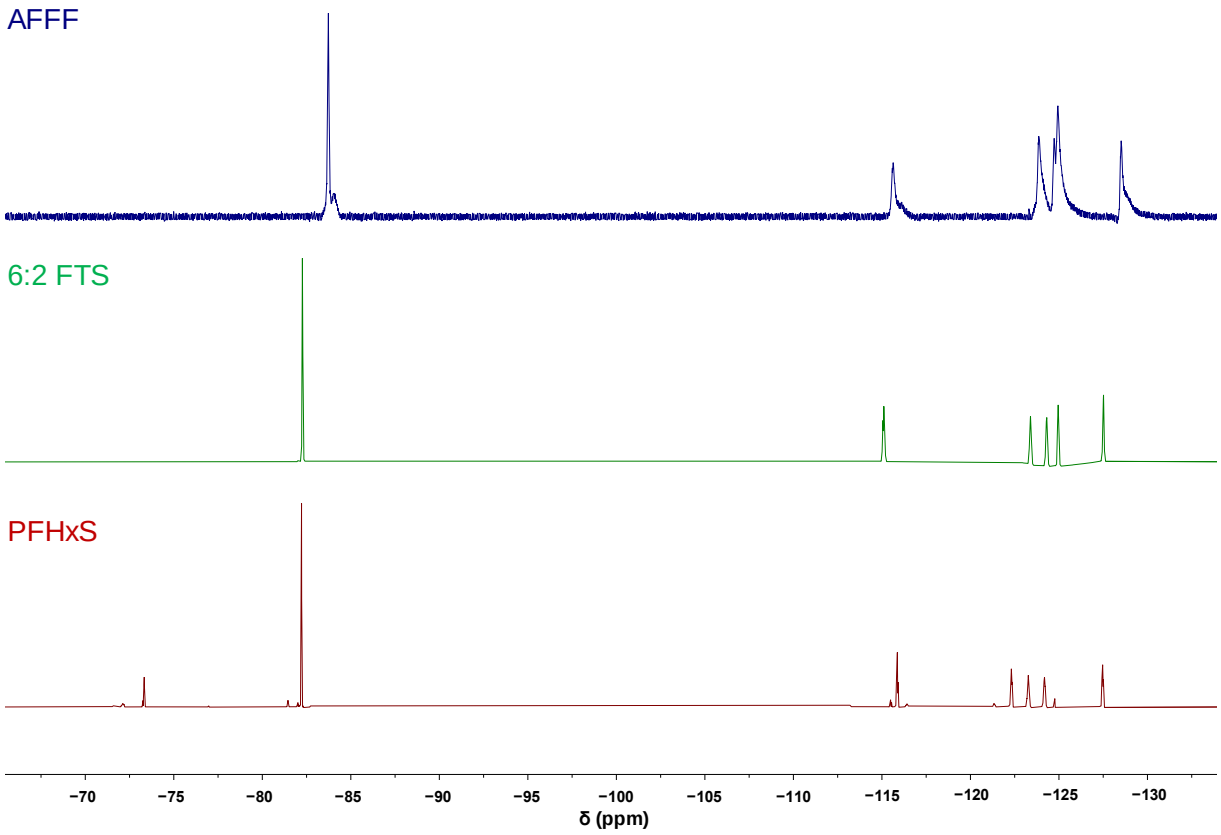

Fig. S10. ^{19}F NMR spectra (in D_2O) for AFFF and two $C_6F_{13}-$ based PFAS (bulk chemicals used as received). The resonance pattern of AFFF resembled more with 6:2 FTS. More convincing evidence for the dominance of $C_6F_{13}-$ telomer structure in AFFF is the formation of PFCA mixtures upon EO treatment.

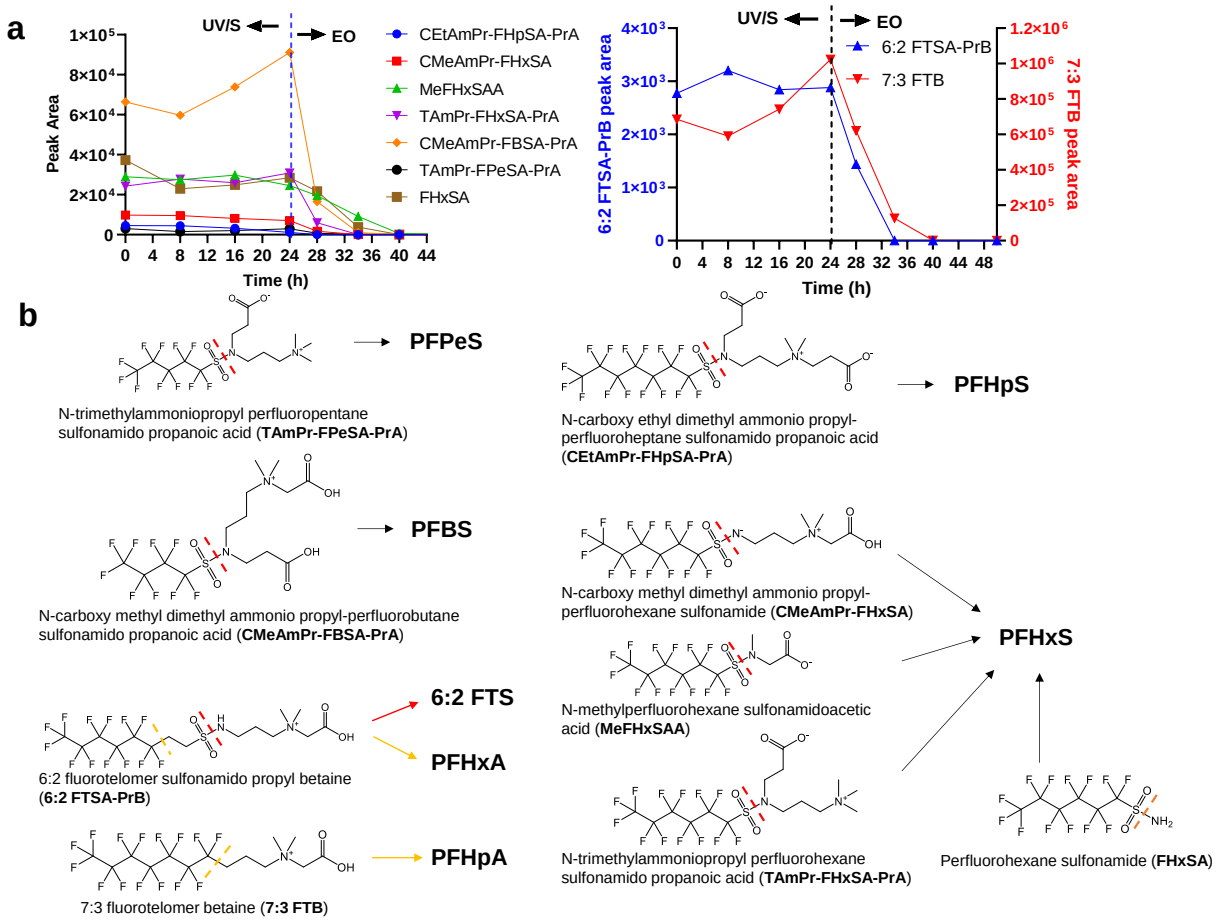

Fig. S 11. **(a)** Variation of Q-ToF-MS peak areas of precursors as functions of reaction time in the UV/S−EO treatment process. **(b)** Basic bond cleavage patterns of precursors that lead to the formation of target PFAS. The red and yellow dash lines indicate the sites of dealkylation and S-N bond cleavage, respectively. Other pathways with deeper defluorination are also possible.

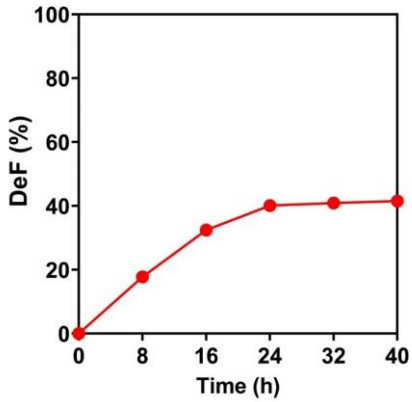

Fig. S12. Defluorination efficiency profile in the UV/S treatment of AFFF (1 to 100 dilution by DI water; [TF] = 103 mg/L, $[Na_2SO_3]_0$ = 100 mM; pH was adjusted to 12 by NaOH).

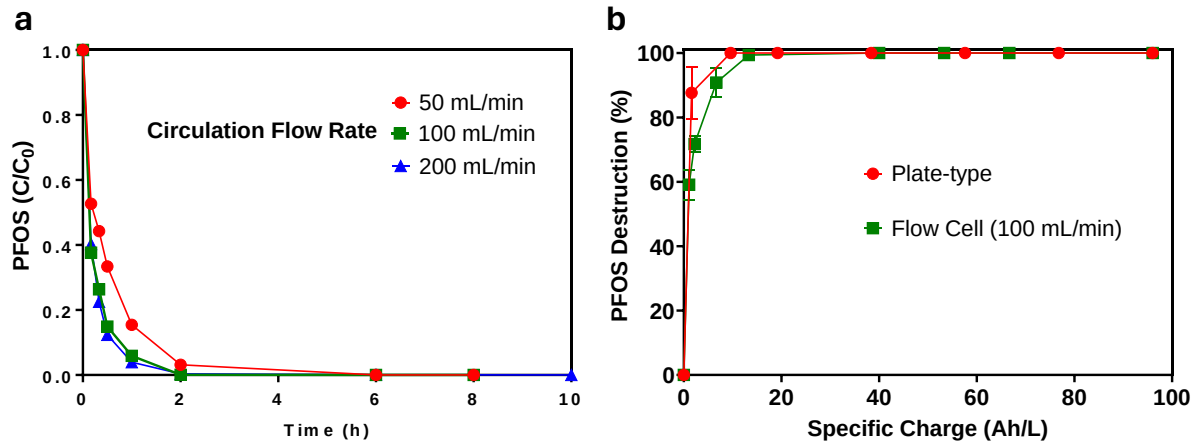

Fig. S13. (a) Optimization of the circulation flow rate of the flow cell for the EO treatment of PFOS (25 μM in 100 mM Na_2SO_4). (b) comparison of PFOS destruction performance between batch reaction and flow cell reactor based on the specific charge. Data are presented as mean values of triplicates ± standard deviation.

It is important to know that we use a commercial flow cell (Element Six) with electrode spacing (0.8 cm) and cell configuration already optimized for industrial wastewater treatment. The flow cell was operated at 5 A. The rationale for selecting this current was provided in the Method section of the manuscript. With most of the parameters and cell configuration pre-fixed, we only optimized the circulation flow rate. As shown in **Fig. S13a**, the increase in flow rate from 50 to 100 mL/min promoted PFOS destruction due to the enhanced mass transfer. However, a flow rate higher than 100 mL/min did not further benefit the reaction. Therefore, the optimized flow rate was determined as 100 mL/min.

Due to the difference in operation mode, applied current, and treatment capacity, it is reasonable to compare the PFOS destruction performance of the two systems on the scale of specific charge (Ah/L). This is a comprehensive descriptor to represent the current (A) and duration (h) required to treat per liter of water. As shown in **Fig. S13b**, the comparison indicates that the optimized flow-cell and batch reactor have comparable PFAS destruction performance. The destruction of PFOS was achieved when a specific charge was larger than 20 Ah/L, corresponding to a treatment duration of 1.7 and 3 h for the plate type (**Fig. 1**) and flow-cell reactor (**Fig. S13a**), respectively.

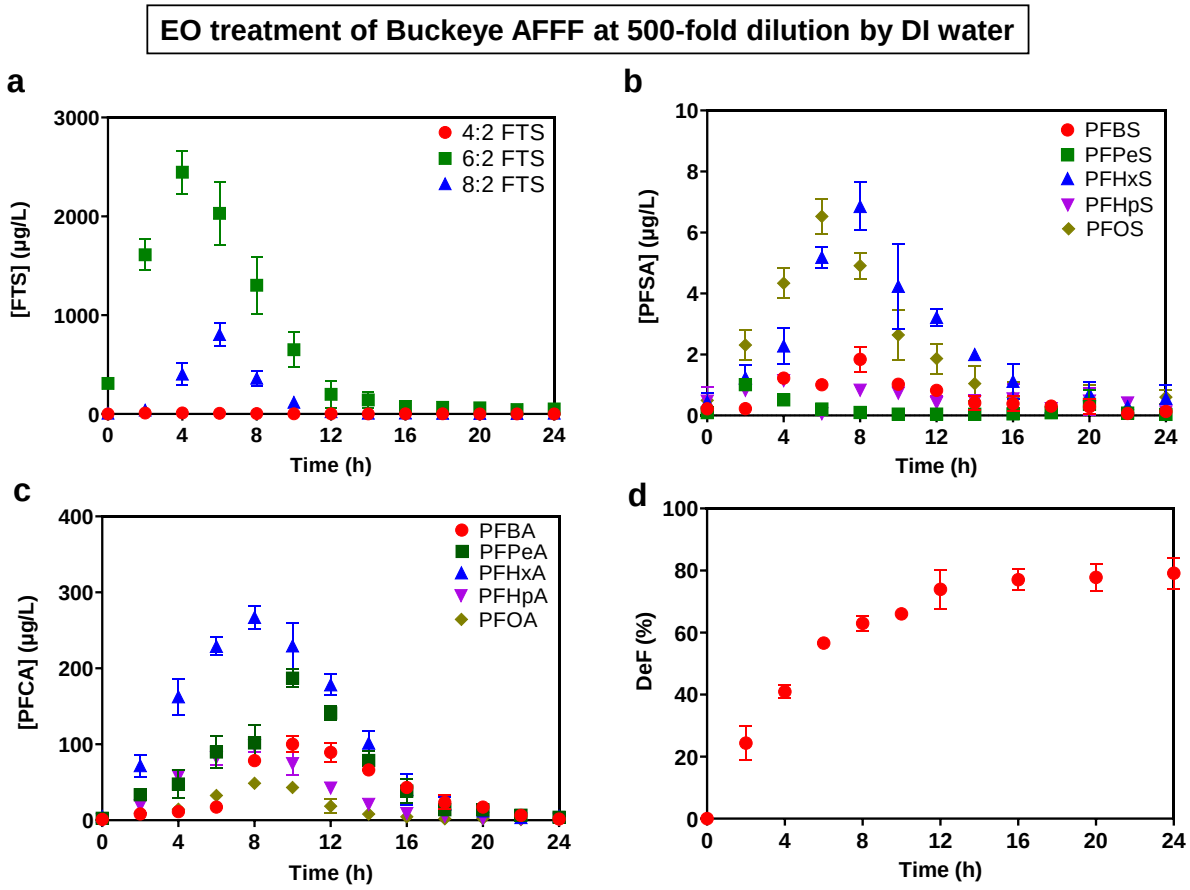

Fig. S14. Profiles of (a) FTS, (b) PFCA, (c) PFSA, and (d) defluorination plotted against reaction time in the EO treatment of AFFF (1 to 500 dilution by DI water; [TF] = 21 mg/L). Data are presented as mean values of triplicates ± standard deviation. The diluted AFFF was amended by 100 mM Na_2SO_4 as a supporting electrolyte. The EO treatment was conducted in a BDD flow cell at a current of 5 A. The resultant cell voltage is 25 V.

The EO treatment of 100-fold diluted Buckeye AFFF was impractical due to the formation of a thick and long-lasting foam layer (Fig. S2). Thus, the tests were conducted to treat 500-fold diluted AFFF. Concentrations of FTS, PFCAs, and PFSAs increased in the first 8 h of electrolysis due to the breakdown of precursors and then destroyed after 24 h (Figs. S14a-c). The defluorination by EO plateaued at 78% (Fig. S14d). As a comparison, UV/S-EO treatment of 500-fold diluted AFFF readily achieved ~100% defluorination (see main article). Therefore, it can be concluded that the UV/S-EO tandem process is the best workflow, outperforming EO or UV/S alone.

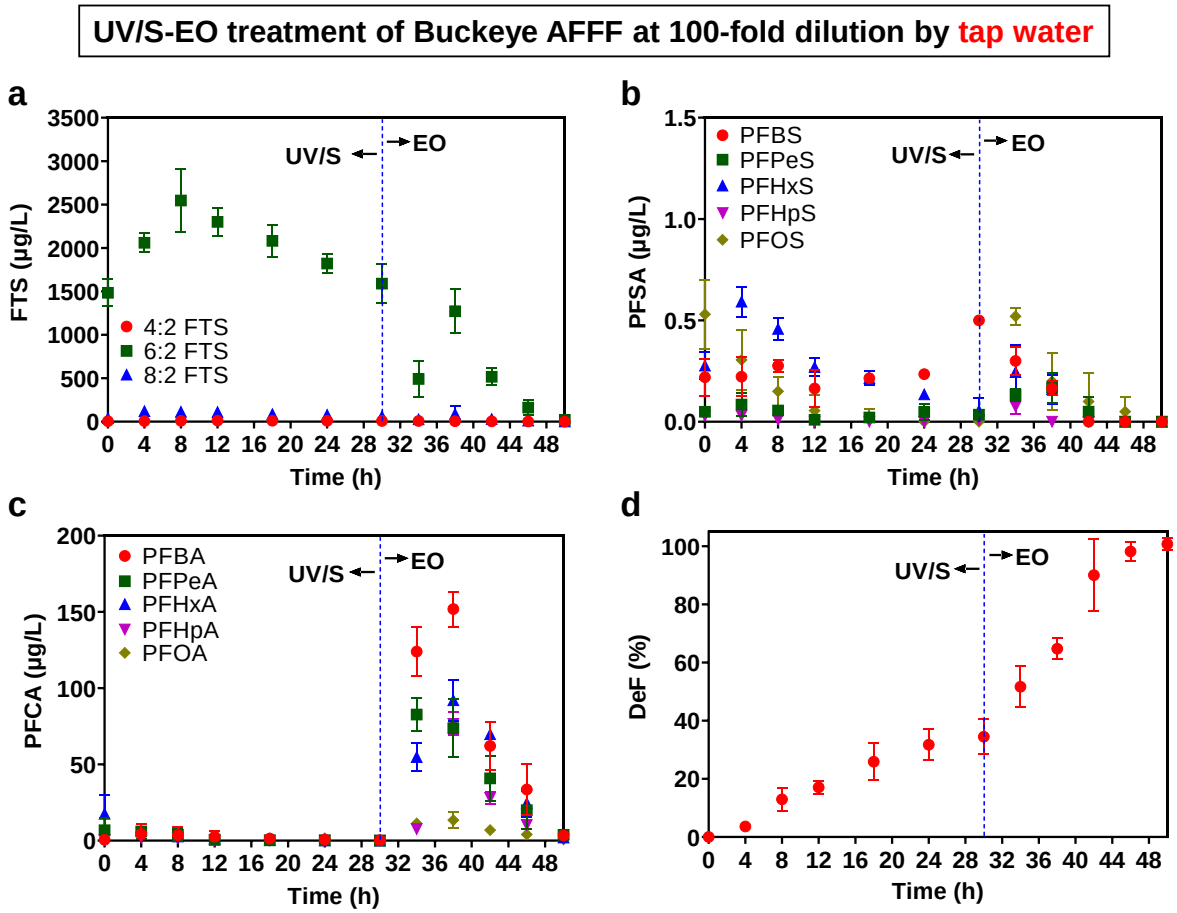

Fig. S15. Profiles of (a) FTS, (b) PFCA, (c) PFSA, and (d) defluorination plotted against reaction time in the UV/S−EO treatment of Buckeye AFFF (1 to 100 dilution by tap water). Data are presented as mean values of triplicates ± standard deviation. Before the UV/S reaction, diluted AFFF was amended by 100 mM Na_2SO_3 and pH was adjusted to 12 by NaOH. The added Na_2SO_3 provides sufficient conductivity for the following EO treatment. Therefore, no chemical addition was required before EO treatment. The EO treatment was conducted in a BDD flow cell at a current of 5 A. The average cell voltage is 25 V.

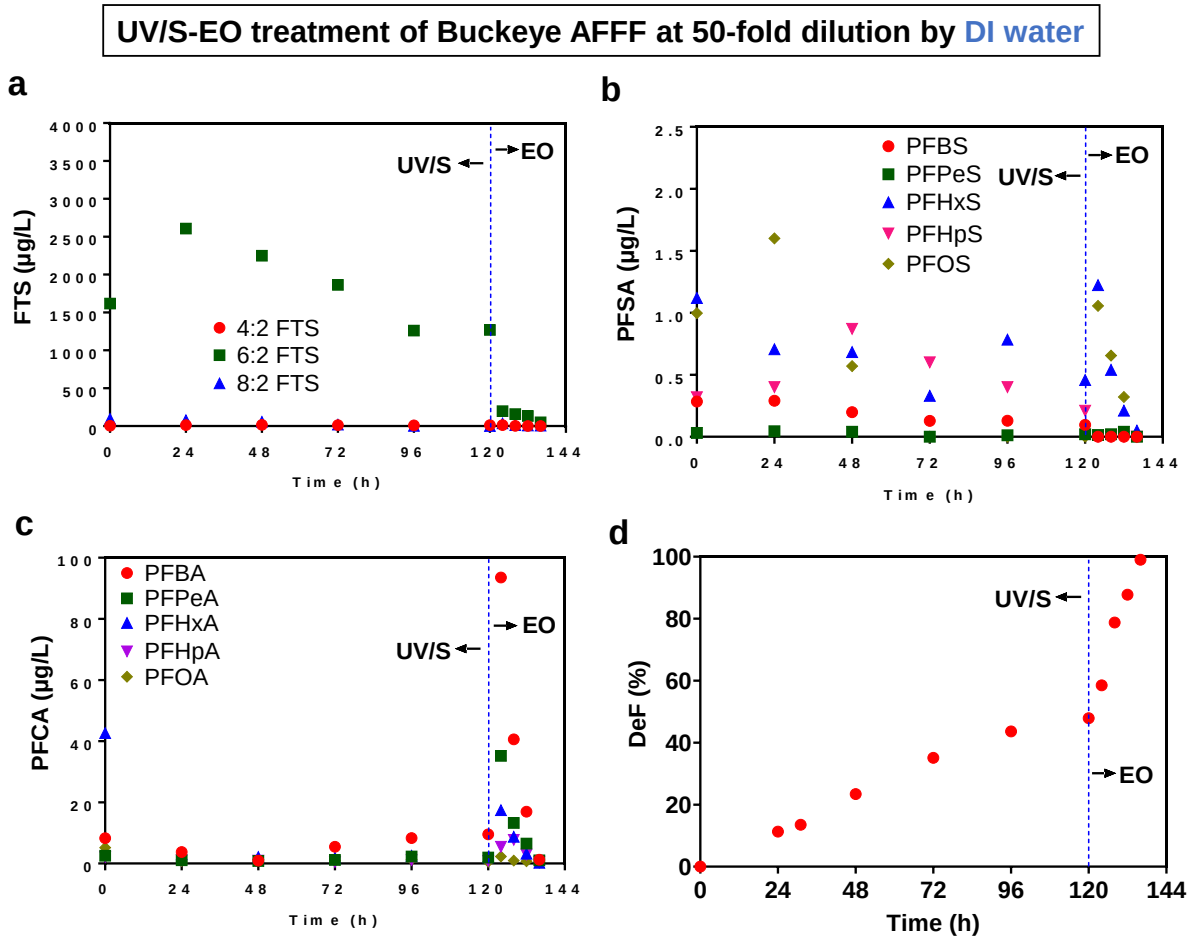

Fig. S16. Profiles of (a) FTS, (b) PFSA, (c) PFCA, and (d) defluorination plotted against reaction time in the UV/S−EO treatment of Buckeye AFFF (1 to 50 dilution by DI water). Data are presented as mean values of triplicates ± standard deviation. Before the UV/S reaction, diluted AFFF was amended by 100 mM Na_2SO_3 and pH was adjusted to 12 by NaOH. The added Na_2SO_3 provides sufficient conductivity for the following EO treatment. Therefore, no chemical addition was required before EO treatment. The EO treatment was conducted in a BDD flow cell at a current of 5 A. The average cell voltage is 25 V.

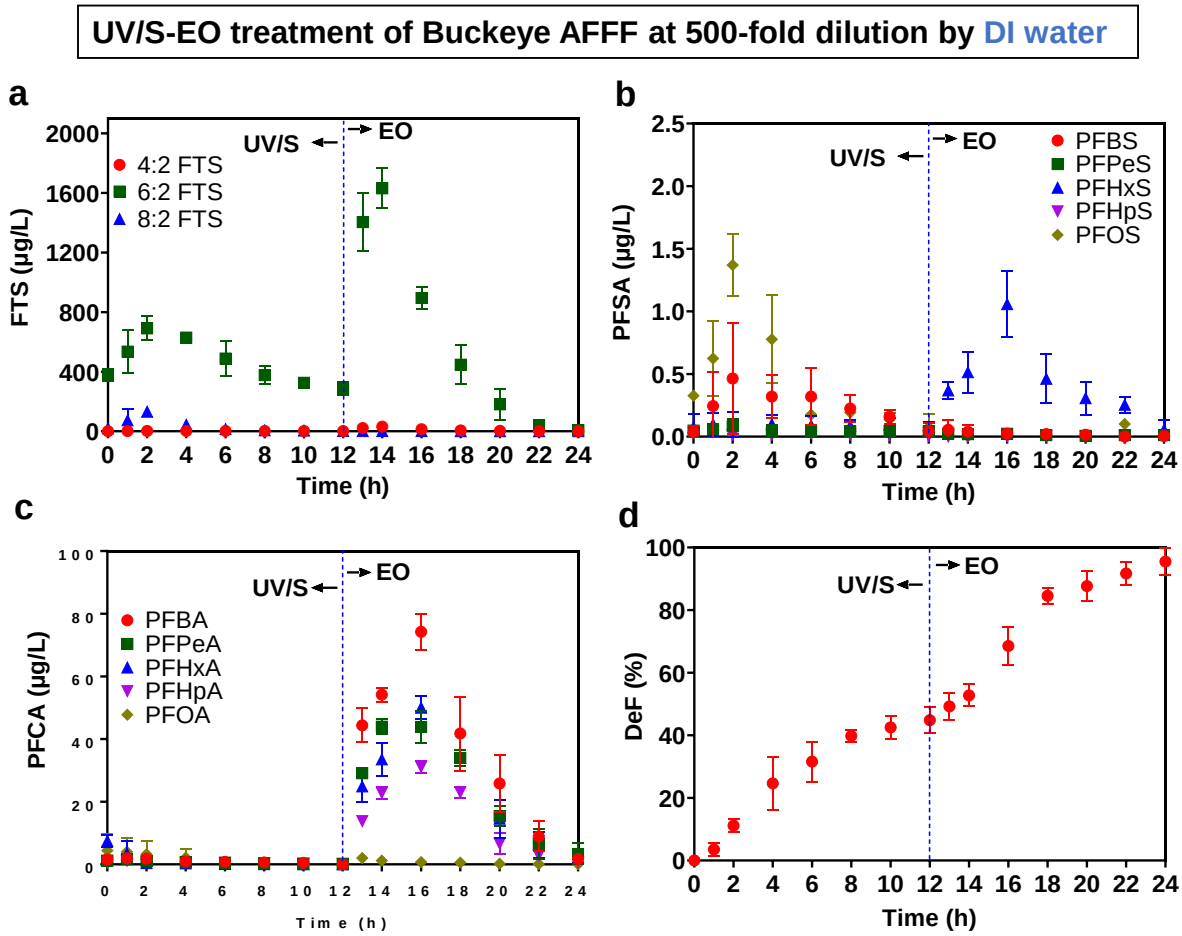

Fig. S17. Profiles of (a) FTS, (b) PFSA, (c) PFCA, and (d) defluorination plotted against reaction time in the UV/S−EO treatment of 500-fold diluted Buckeye AFFF by DI water. Data are presented as mean values of triplicates ± standard deviation. Before the UV/S reaction, diluted AFFF was amended by 10 mM Na_2SO_3 and pH was adjusted to 12 by NaOH. After UV/S treatment, 90 mM Na_2SO_4 was spiked in water to provide sufficient conductivity in EO treatment. The EO treatment was conducted in a BDD flow cell at a current of 5 A. The average cell voltage is 25 V.

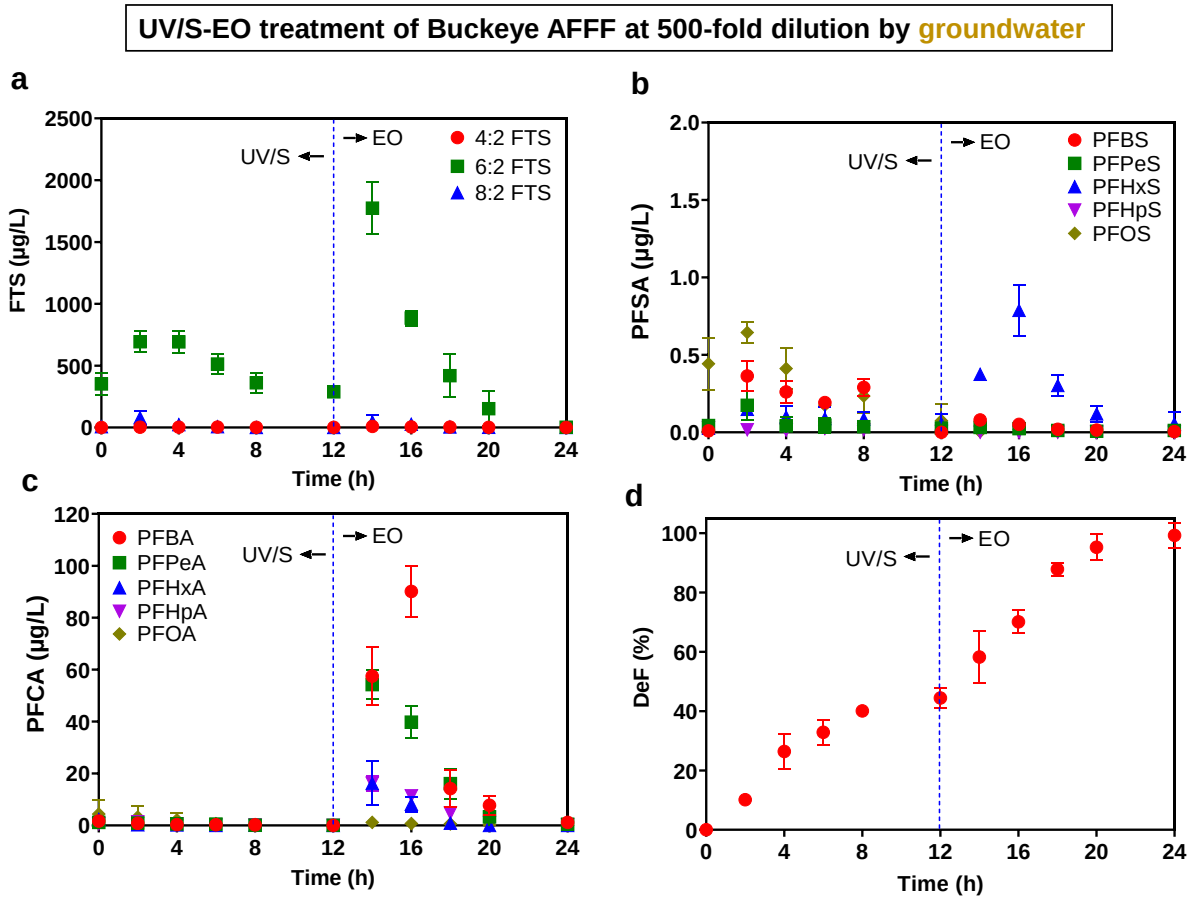

Fig. S18. Profiles of (a) FTS, (b) PFSA, (c) PFCA, and (d) defluorination plotted against reaction time in the UV/S−EO treatment of 500-fold diluted Buckeye AFFF by groundwater. Data are presented as mean values of triplicates ± standard deviation. Before the UV/S reaction, diluted AFFF was amended by 10 mM Na_2SO_3 and pH was adjusted to 12 by NaOH. After UV/S treatment, 90 mM Na_2SO_4 was spiked in water to provide sufficient conductivity in EO treatment. The EO treatment was conducted in a BDD flow cell at a current of 5 A. The average cell voltage is 25 V.

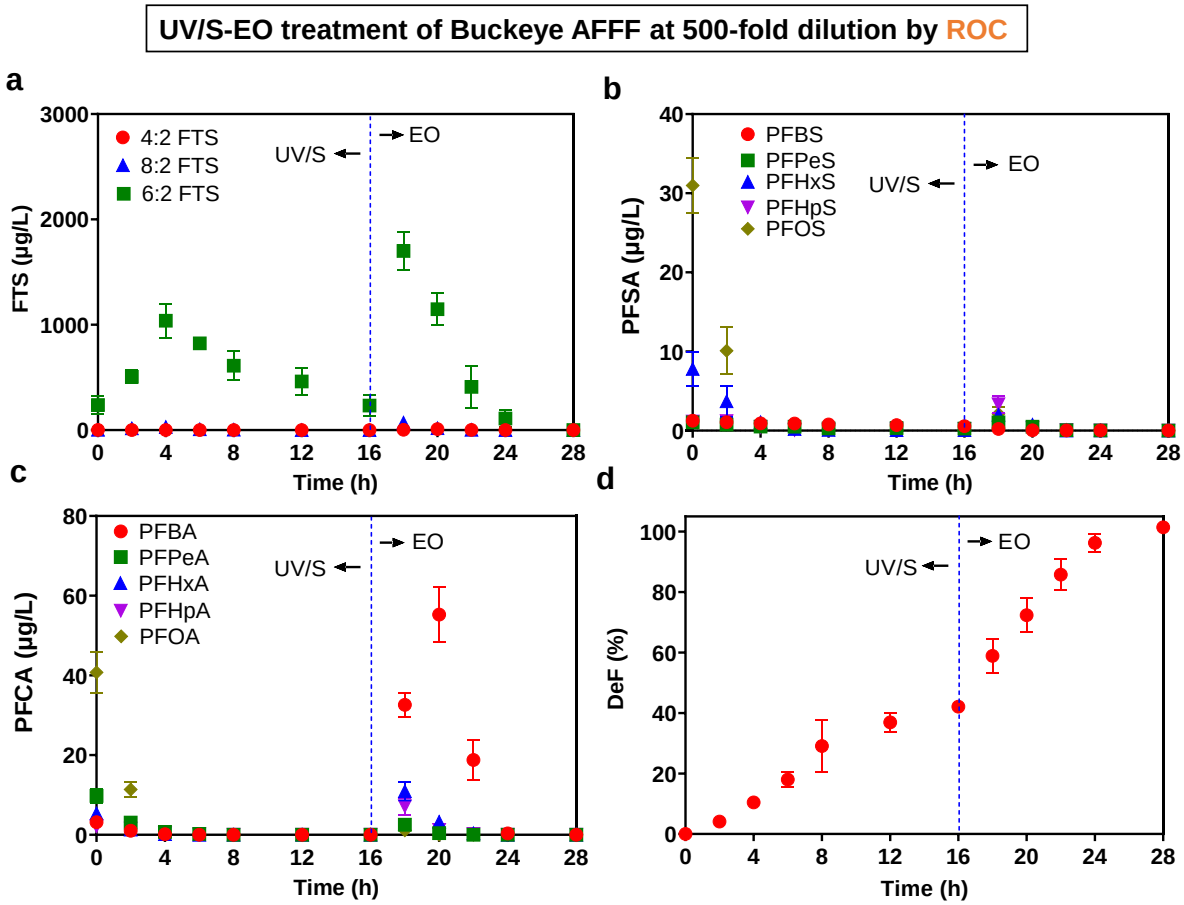

Fig. S19. Profiles of (a) FTS, (b) PFSA, (c) PFCA, and (d) defluorination plotted against reaction time in the UV/S−EO treatment of 500-fold diluted Buckeye AFFF by reversed osmosis concentrate (ROC). Data are presented as mean values of triplicates ± standard deviation. Before the UV/S treatment, diluted AFFF was amended by 10 mM Na_2SO_3 and pH was adjusted to 12 by NaOH. After UV/S treatment, 90 mM Na_2SO_4 was spiked in water to provide sufficient conductivity in EO treatment. The EO treatment was conducted in a BDD flow cell at a current of 5 A. The average cell voltage is 22 V.

It is important to note that the ROC derived from a site-remediation project already contains PFSAs and PFCAs. These existing PFAS elevated the time-zero concentrations of PFSAs and PFCAs compared with diluted AFFF by DI water and groundwater.

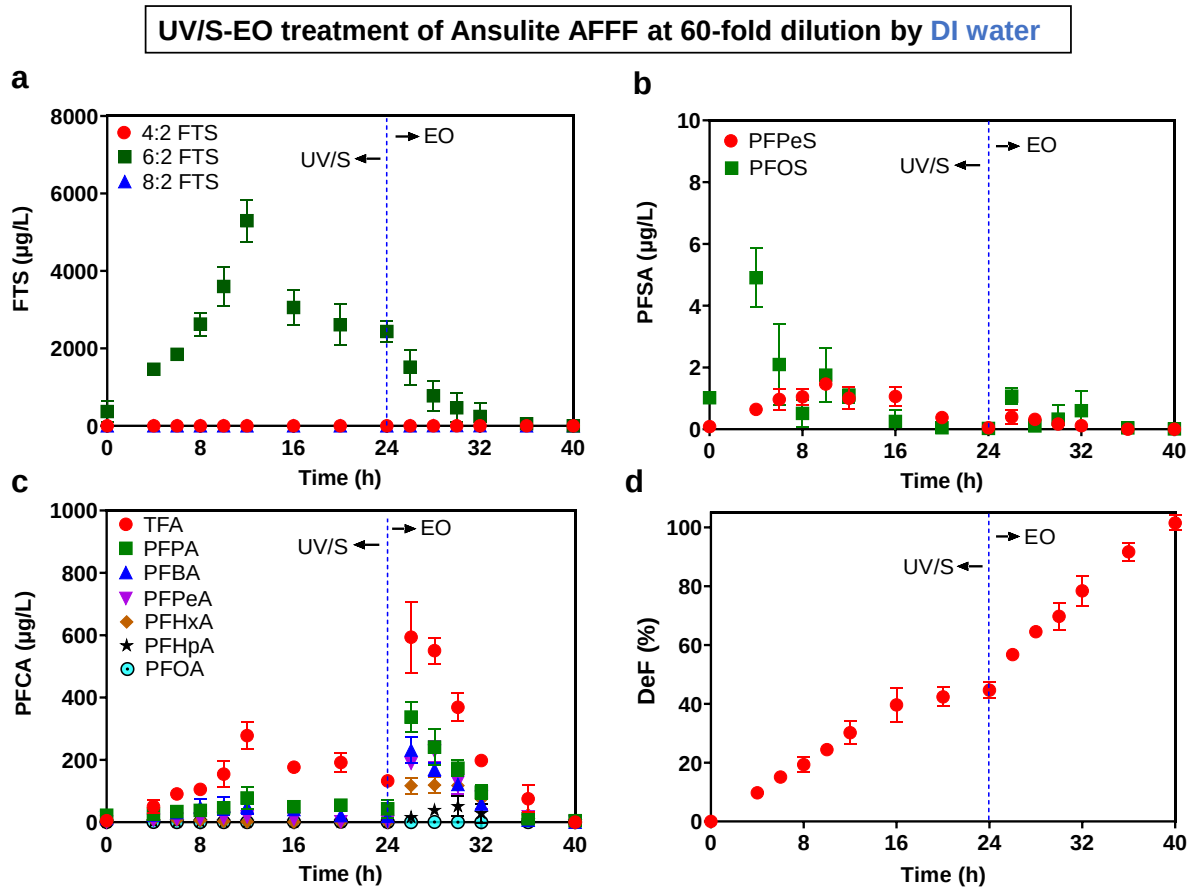

Fig. S20. Profiles of (a) FTS, (b) PFSA, (c) PFCA, and (d) defluorination plotted against reaction time in the UV/S-EO treatment of Ansulite AFFF (1 to 60 dilution by DI water; [TF] = 102 mg/L). Data are presented as mean values of triplicates ± standard deviation. Before the UV/S reaction, diluted AFFF was amended by 10 mM Na_2SO_3 and pH was adjusted to 12 by NaOH. The added Na_2SO_3 provides sufficient conductivity for the following EO treatment. Therefore, no chemical addition was required before EO treatment. The EO treatment was conducted in a BDD flow cell at a current of 5 A. The resultant cell voltage is 25 V.

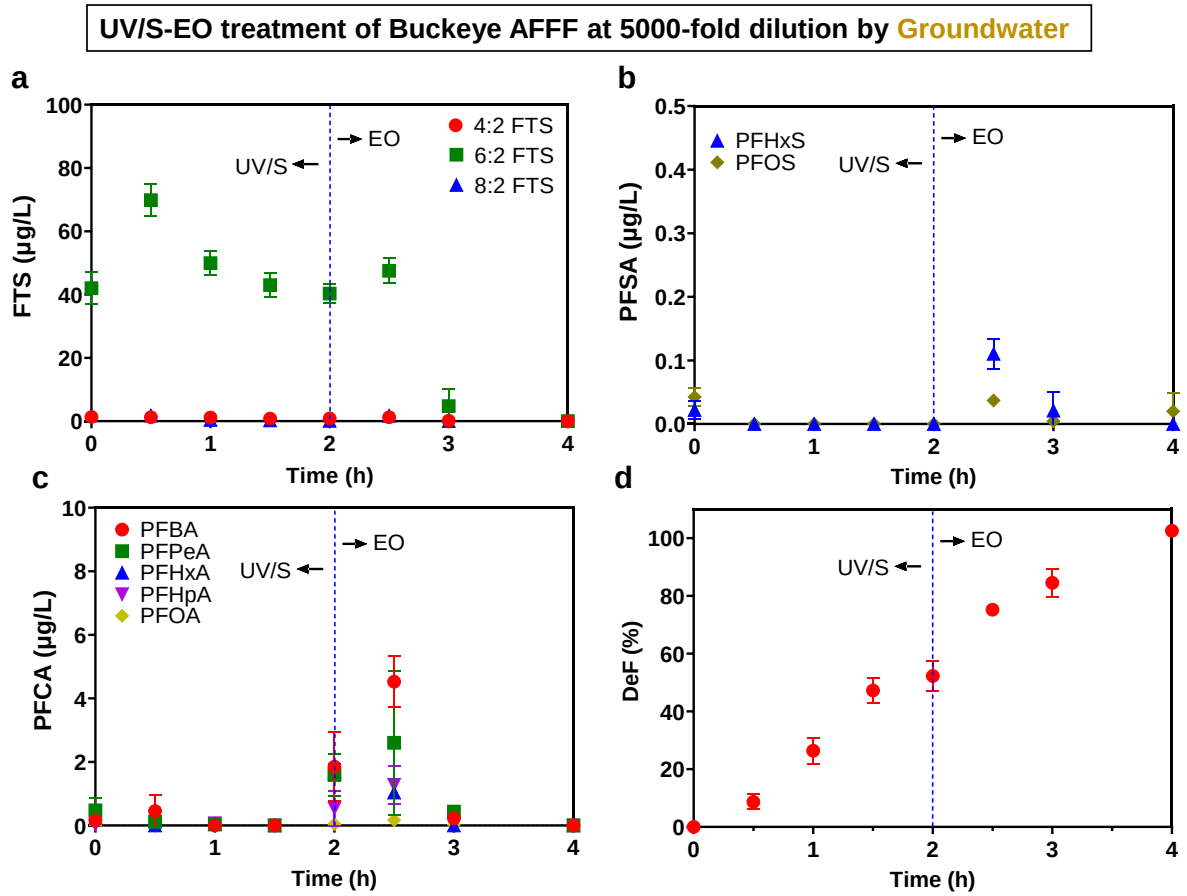

Fig. S21. Profiles of (a) FTS, (b) PFSA, (c) PFCA, and (d) defluorination plotted against reaction time in the UV/S-EO treatment of AFFF (1 to 5000 dilution by groundwater; [TF] = 2 mg/L). Data are presented as mean values of triplicates ± standard deviation. Before the UV/S treatment, diluted AFFF was amended by 10 mM Na_2SO_3 and pH was adjusted to 12 by NaOH. After UV/S treatment, 90 mM Na_2SO_4 was spiked in water to provide sufficient conductivity in EO treatment. The EO treatment was conducted in a BDD flow cell at a current of 5 A. The resultant cell voltage is 25 V.

References

(1) Shi, H.; Wang, Y.; Li, C.; Pierce, R.; Gao, S.; Huang, Q. Degradation of Perfluorooctanesulfonate by Reactive Electrochemical Membrane Composed of Magnéli Phase Titanium Suboxide. *Environ. Sci. Technol.* **2019**, *53* (24), 14528–14537. https://doi.org/10.1021/acs.est.9b04148.

(2) Frisch, M. J.; Trucks, G. W.; Schlegel, H. B.; Scuseria, G. E.; Robb, M. A.; Cheeseman, J. R.; Scalmani, G.; Barone, V.; Petersson, G. A.; Nakatsuji, H.; Li, X.; Caricato, M.; Marenich, A. V.; Bloino, J.; Janesko, B. G.; Gomperts, R.; Mennucci, B.; Hratchian, H. P.; Ortiz, J. V.; Izmaylov, A. F.; Sonnenberg, J. L.; Williams; Ding, F.; Lipparini, F.; Egidi, F.; Goings, J.; Peng, B.; Petrone, A.; Henderson, T.; Ranasinghe, D.; Zakrzewski, V. G.; Gao, J.; Rega, N.; Zheng, G.; Liang, W.; Hada, M.; Ehara, M.; Toyota, K.; Fukuda, R.; Hasegawa, J.; Ishida, M.; Nakajima, T.; Honda, Y.; Kitao, O.; Nakai, H.; Vreven, T.; Throssell, K.; Montgomery Jr., J. A.; Peralta, J. E.; Ogliaro, F.; Bearpark, M. J.; Heyd, J. J.; Brothers, E. N.; Kudin, K. N.; Staroverov, V. N.; Keith, T. A.; Kobayashi, R.; Normand, J.; Raghavachari, K.; Rendell, A. P.; Burant, J. C.; Iyengar, S. S.; Tomasi, J.; Cossi, M.; Millam, J. M.; Klene, M.; Adamo, C.; Cammi, R.; Ochterski, J. W.; Martin, R. L.; Morokuma, K.; Farkas, O.; Foresman, J. B.; Fox, D. J. Gaussian 16 Rev. C.01, 2016.

(3) Li, X.; Ma, J.; Liu, G.; Fang, J.; Yue, S.; Guan, Y.; Chen, L.; Liu, X. Efficient Reductive Dechlorination of Monochloroacetic Acid by Sulfite/UV Process. *Environ. Sci. Technol.* **2012**, *46* (13), 7342–7349. https://doi.org/10.1021/es3008535.

(4) Tenorio, R.; Liu, J.; Xiao, X.; Maizel, A.; Higgins, C. P.; Schaefer, C. E.; Strathmann, T. J. Destruction of Per- and Polyfluoroalkyl Substances (PFASs) in Aqueous Film-Forming Foam (AFFF) with UV-Sulfite Photoreductive Treatment. *Environ. Sci. Technol.* **2020**, *54* (11), 6957–6967. https://doi.org/10.1021/acs.est.0c00961.

(5) Li, H.; Quispe-Cardenas, E.; Yang, S.; Yin, L.; Yang, Y. Electrosynthesis of >20 g/L H2O2 from Air. *ACS EST Eng.* **2022**, *2* (2), 242–250. https://doi.org/10.1021/acsestengg.1c00366.

(6) Schaefer, C. E.; Choyke, S.; Ferguson, P. L.; Andaya, C.; Burant, A.; Maizel, A.; Strathmann, T. J.; Higgins, C. P. Electrochemical Transformations of Perfluoroalkyl Acid (PFAA) Precursors and PFAAs in Groundwater Impacted with Aqueous Film Forming Foams. *Environ. Sci. Technol.* **2018**, *52* (18), 10689–10697.

(7) E. Schaefer, C.; Tran, D.; Fang, Y.; Jeong Choi, Y.; P. Higgins, C.; J. Strathmann, T. Electrochemical Treatment of Poly- and Perfluoroalkyl Substances in Brines. *Environ. Sci. Water Res. Technol.* **2020**, *6* (10), 2704–2712. https://doi.org/10.1039/D0EW00377H.

(8) Luo, Y.; Khoshyan, A.; Al Amin, M.; Nolan, A.; Robinson, F.; Fenstermacher, J.; Niu, J.; Megharaj, M.; Naidu, R.; Fang, C. Ultrasound-Enhanced Magnéli Phase Ti4O7 Anodic Oxidation of per- and Polyfluoroalkyl Substances (PFAS) towards Remediation of Aqueous Film Forming Foams (AFFF). *Sci. Total Environ.* **2023**, *862*, 160836. https://doi.org/10.1016/j.scitotenv.2022.160836.

(9) Singh, R. K.; Multari, N.; Nau-Hix, C.; Anderson, R. H.; Richardson, S. D.; Holsen, T. M.; Mededovic Thagard, S. Rapid Removal of Poly- and Perfluorinated Compounds from Investigation-Derived Waste (IDW) in a Pilot-Scale Plasma Reactor. *Environ. Sci. Technol.* **2019**, *53* (19), 11375–11382. https://doi.org/10.1021/acs.est.9b02964.

(10) Hao, S.; Choi, Y.-J.; Wu, B.; Higgins, C. P.; Deeb, R.; Strathmann, T. J. Hydrothermal Alkaline Treatment for Destruction of Per- and Polyfluoroalkyl Substances in Aqueous Film-Forming Foam. *Environ. Sci. Technol.* **2021**, *55* (5), 3283–3295. https://doi.org/10.1021/acs.est.0c06906.

(11) Pinkard, B. R. Aqueous Film-Forming Foam Treatment under Alkaline Hydrothermal Conditions. *J. Environ. Eng.* **2022**, *148* (2), 05021007. https://doi.org/10.1061/(ASCE)EE.1943-7870.0001974.
(12) Zhang, Y.; Yang, Y.; Yang, S.; Quispe-Cardenas, E.; Hoffmann, M. R. Application of Heterojunction Ni–Sb–SnO2 Anodes for Electrochemical Water Treatment. *ACS EST Eng.* **2021**, *1* (8), 1236–1245. https://doi.org/10.1021/acsestengg.1c00122.